

## Correlation of aerodynamic forces on an inclined circular cylinder

Shaohong Cheng<sup>†</sup> and Hiroshi Tanaka<sup>‡</sup>

Department of Civil Engineering, University of Ottawa, 161 Louis Pasteur, Ottawa, ON K1N 6N5 Canada  
(Received December 1, 2003, Accepted December 1, 2004)

**Abstract.** Divergent galloping-like motion of a dry inclined cable has been observed in a limited number of experimental studies, which, due to the uncertainties in its onset conditions, has induced serious concerns in the bridge stay cable design. A series of dynamic and static model wind tunnel tests have been carried out to confirm the existence of the phenomenon and clarify its excitation mechanism. The present paper focuses on exploring the spatial flow structure around an inclined cable. The pattern of resultant aerodynamic forces acting at different longitudinal locations of the model and the spatial correlation of the forces are examined. The results lead one step closer in revealing the physical nature of the phenomenon.

**Keywords:** cable aerodynamics; inclined circular cylinder; dry inclined cable galloping; correlation; Reynolds number.

---

### 1. Introduction

The flow field around a typical stay cable on cable-stayed bridges has strong three-dimensional characteristics due to its orientation. As a result, some distinct types of wind-induced cable vibration specifically related to inclined cables, i.e., rain-wind induced vibration, high-speed vortex excitation and dry inclined cable galloping, have been identified in recent years both in field (Hikami 1986, Virlogeux 1998, Irwin, *et al.* 1999) and in wind tunnel tests (Saito, *et al.* 1994, Miyata, *et al.* 1994, Honda, *et al.* 1995, Matsumoto, *et al.* 1995, 1998, 2001, Main and Jones 1999). The last issue, though has never been observed explicitly on the bridge site, occurred in a limited number of experimental studies (Saito, *et al.* 1994, Miyata, *et al.* 1994, Honda, *et al.* 1995, Matsumoto, *et al.* 1995, Cheng, *et al.* 2002). The phenomenon was found to have the same response characteristics as classical galloping. It was sensitive to the physical conditions and therefore difficult to be reproduced. Also, it is interesting to note that based on the model size and testing wind speed, the divergent cable motion reported by Saito, *et al.* (1994) and Matsumoto, *et al.* (1995) occurred in the sub-critical Reynolds number range, whereas that observed by the authors (Cheng, *et al.* 2002) occurred in the critical Reynolds number range, within which the characteristics of aerodynamic forces change drastically. Due to the uncertainties in its onset conditions, it causes serious concerns in the bridge stay cable design and has become one of the most problematic issues in the field today. In order to lift the mysterious veil of this unfavorable cable behaviour and clarify its

---

<sup>†</sup> Post Doctoral Research Fellow

<sup>‡</sup> Professor, E-mail: [htanaka@uottawa.ca](mailto:htanaka@uottawa.ca)

generation mechanism, a collaborative research project was initiated by the University of Ottawa, National Research Council Canada (NRCC), and Rowan Williams Davies and Irwin Inc.. In the present paper, the experimental work and the major results of the study obtained so far are briefly reviewed first as a base for further discussion. Focus will be placed on studying the flow-induced forces on an inclined cable, particularly the pattern of resultant aerodynamic forces acting at different longitudinal locations of the model, the characteristics of span-wise correlation of lift force including its variation against wind speed and model orientation in the sub-critical and critical Reynolds number range, and the spatial flow structure around the inclined cable model. The results lead one step closer in revealing the physical nature of the phenomenon.

## 2. Experimental work and previous results

A series of dynamic and static model wind tunnel tests have been conducted. A 6.7 m long 2D sectional full-scale cable model was investigated in the dynamic tests as shown in Fig. 1(a). The model setup, testing programs and observed phenomena are described in details by Cheng, *et al* (2002, 2003a, 2003b). The divergent motion was successfully observed at a model setup equivalent to a real bridge stay cable inclined and yawed both with  $45^\circ$  against the mean wind direction. The observed critical wind speed was 32 m/s, which corresponds to a reduced wind speed of 134. Based on model diameter and mean wind speed, the equivalent Reynolds number is  $3.33 \times 10^5$ , which is within the critical range. When the instability occurred, the model had smooth surface condition and very low damping corresponding to Scruton number of 11. In the scope of current study, the Scruton number is defined as  $m\delta/\rho D^2$ , where  $m$  is cable mass per unit length,  $\delta$  is logarithmic decrement,  $\rho$  is air density, and  $D$  is cable diameter. The response characteristics were found to be the same as galloping. During the tests, it was observed that once wind speed exceeded the critical value of 32 m/s, the amplitude of the motion increased by four times within 480 cycles to a recorded peak-to-peak amplitude close to  $1D$ , where  $D$  is the cable diameter. It tended to grow



(a) Dynamic model in the NRCC 3m x 6m  
Propulsion wind tunnel



(b) Static model in the NRCC 2m x 3m wind tunnel

Fig. 1 Experimental setups

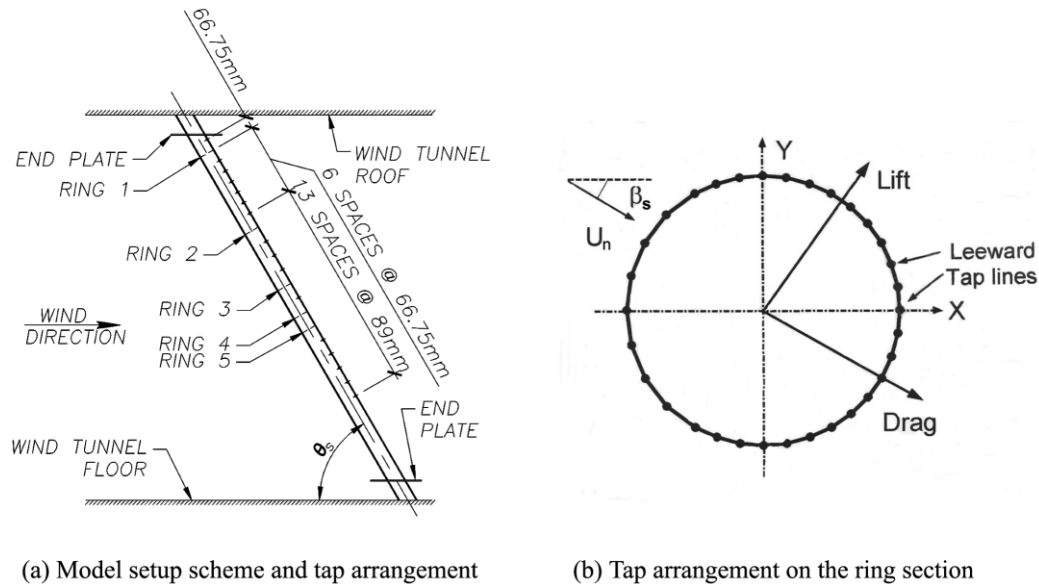


Fig. 2 Static model test setup and pressure tap arrangement

further, but had to be manually suppressed due to the restrictions of model setup.

For a better understanding of the generation mechanism, the critical onset conditions and the possibility of occurrence of this instability on real cable-stayed bridges, aerodynamic information of flow field around an inclined cable is required. Therefore, time-dependent surface pressure of a stationary rigid circular cylinder model was measured as a continuing phase in the 2 m (H) × 3 m (W) wind tunnel at IAR/NRCC, as shown in Fig. 1(b). A total number of 192 pressure taps were installed on the model. Five pressure tap rings, with 32 taps in each ring, were arranged at different longitudinal locations along the model. The plane of each ring was perpendicular to the model axis. In addition, two longitudinal tap lines were installed at the leeward side of the model, with 16 taps on each line. Fig. 2 presents the tap arrangement on the whole model and each ring. Elliptical plates were attached close to both ends of the model to reduce the end effects. The resultant aerodynamic forces acting on different model sections coinciding with the tap ring planes were obtained through integration of pressures sampled simultaneously by all 32 taps on the same ring over tributary areas. Referring to Fig. 2(b), the sectional drag and lift forces within each individual ring plane were calculated by decomposing the resultant force along and perpendicular to the direction of mean wind speed component normal to the model axis.

When modelling wind-induced cable vibration, the relative angles between the directions of wind, cable axis and cable motion should be consistent with the full scale case. Considering the constraints of the possible model motion direction in the dynamic and static tests, the static model would be at its critical orientation when set up with a vertical inclination angle of  $54.7^\circ$  and a yaw angle of  $30^\circ$  against the mean wind direction. The combination of these two angles gives the same cable-wind relative angle, i.e., the effective wind angle of attack, as that in the dynamic tests where the divergent motion occurred. Because varying either the vertical inclination angle or horizontal yaw angle of the model would cause a change in the cable-wind relative angle, in the static tests, surface pressure of the model was sampled with combination of fixed inclination angle and varying

yaw angle to achieve different cable-wind relative angle.

Since the Reynolds number is kept the same in the dynamic and static tests, the critical wind speed of the static model would expect to be within the range of 50-60 m/s (corresponding to Reynolds number range of  $2.9-3.5 \times 10^5$ ) (Cheng, *et al.* 2003b). Examinations on the characteristics of model aerodynamic forces show that when the model was set up with a vertical angle of  $54.7^\circ$ , within the expected critical ranges of model yaw angle and wind speed, besides the significant decrease of model drag coefficient, its lift coefficient curve is found to have negative slopes against the variation of the angle of attack. The combined effects of these two facts will finally results in negative aerodynamic damping of the structure and lead to a possible mechanism similar to that of the Den Hartog criterion for conventional iced-cable galloping. Further research effort (Cheng, *et al.* 2003c) verifies the validity of applying Den Hartog criterion to explain this unfavourable cable behaviour. The critical onset wind speed of divergent cable motion predicted by the Den Hartog criterion agrees with that observed in the dynamic tests. For a deeper insight into the essence of the phenomenon, the spatial structure of the flow field around an inclined cable needs to be investigated.

### 3. Resultant aerodynamic force

The pattern of air flow field surrounding a cable determines the nature of its wind-induced behaviour. Such effect can be described by resultant aerodynamic force acting on the cable. In this section, the resultant of sectional lift and drag forces in the cross-sectional plane coinciding with that of pressure tap rings at different longitudinal locations of the model is calculated. Refer to Fig. 2(b), the direction angle of the resultant force is measured in a counter-clockwise direction from X-axis, which is the along-wind direction in non-yawed case. By normalizing it with the dynamic pressure and the model diameter, the corresponding resultant force coefficient is obtained.

Preliminary analysis shows that results obtained from Ring 1 are not consistent with those obtained from the other four rings. This could be mainly attributed to the close distance between Ring 1 and the top end plate. Therefore, discussion in the remaining part of the paper will be based on the data from Rings 2-5. Fig. 3 shows the variation of magnitude and direction angle of the resultant force coefficient vector against wind speed when the model is inclined with  $54.7^\circ$  to the horizontal plane. Results at five yaw angles including both the critical cases of  $\beta_s = 29^\circ, 30^\circ, 31^\circ$  and the non-critical cases of  $\beta_s = 20^\circ, 40^\circ$  are presented.

As depicted in Fig. 3, though the magnitude of the resultant coefficient vector of different rings are at the same level, their direction change with both the wind speed and the longitudinal position. When wind speed is lower than 40 m/s, i.e., in the subcritical Reynolds number range, the characteristics of the flow state in terms of separation point, boundary layer etc. vary slightly along the whole model span, which, as reflected in this set of figures, is the fact that the direction angle of different resultant vectors generally agree. The aerodynamic damping of the model at this stage is positive (Cheng, *et al.* 2003c), the cable motion is thus decayed with time. However, when the wind speed increases to 50-60 m/s and the critical Reynolds number is reached, the direction of Ring 2 vector coincides more or less with that of Ring 3, whereas Ring 4 vector is more conformable with that of Ring 5. Since Rings 2 and 3 are arranged in the top part of the model, whereas Rings 4 and 5 are in the bottom part, this means that within this wind speed range, the resultant aerodynamic forces acting on two different longitudinal parts of the cable drive the cable motion in two different directions, with one in the direction angle greater than model yaw angle  $\beta_s$ , and another in the angle smaller than  $\beta_s$ . As a result, it makes the cross-flow effects of these resultant forces less effective.

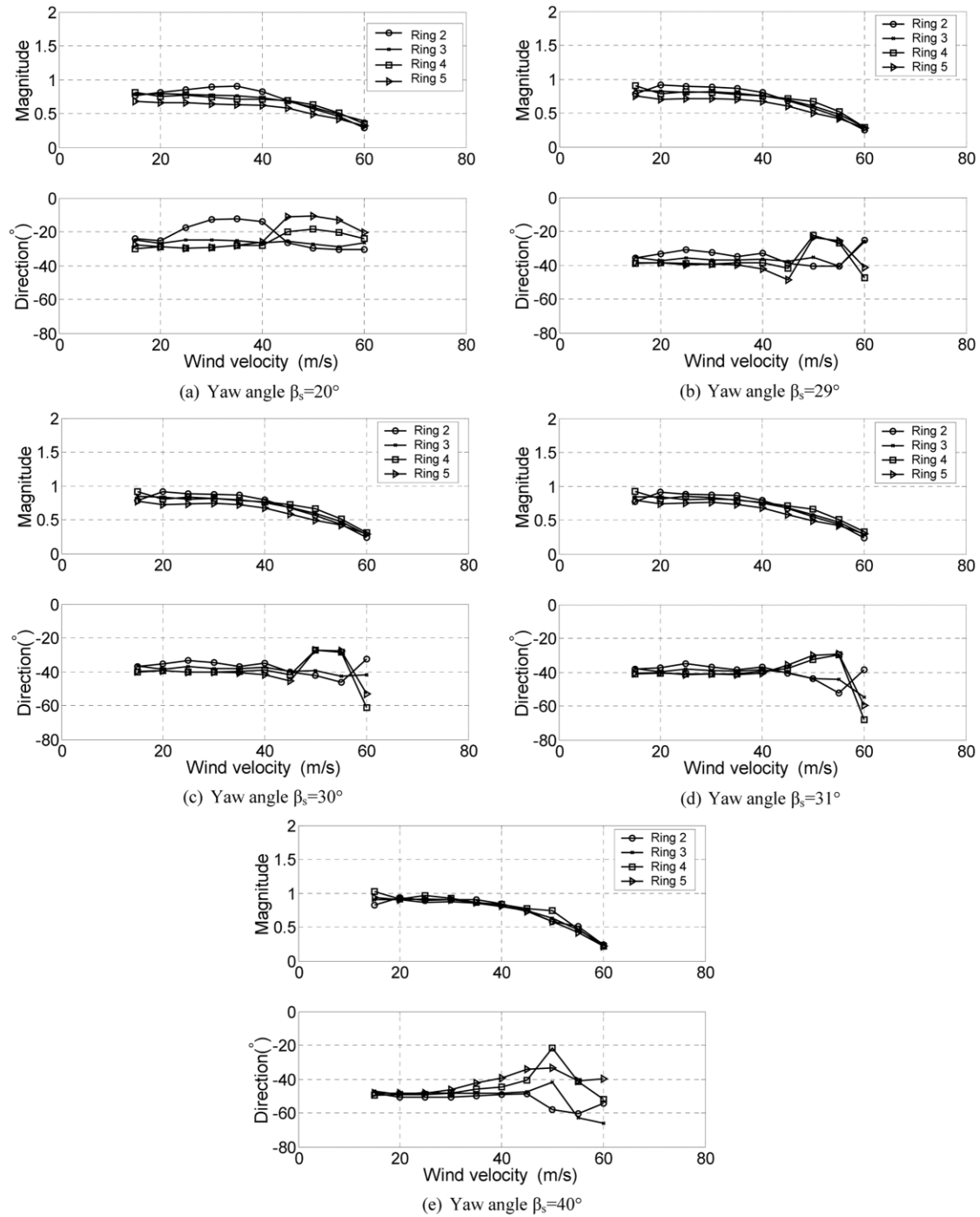


Fig. 3 Resultant force coefficient vector on an inclined cable ( $\theta_s = 54.7^\circ$ )

Further, as shown in Figs. 3(b)-(d), within this wind speed range, when the cable is given a yaw angle in the vicinity of the critical value of  $30^\circ$ , a remarkable “direction angle switch” phenomenon

can be observed. With the increase of wind speed from 55 m/s to 60 m/s, for the group containing resultant vectors of Rings 2 and 3, the direction angles become smaller, whereas for the group containing those of Rings 4 and 5, the direction angles become larger. Thus, there must be a specific wind speed between 55 m/s and 60 m/s at which the directions of all these four resultant force coefficient vectors would coincide and generate greater cross-flow effect. Combining with the results obtained from an earlier study (Cheng, *et al.* 2003c) that  $U = 50\text{--}60$  m/s is the critical wind speed range where the aerodynamic damping of the model is found to be negative, it leads to the fact that because the cross-flow component is in phase with the cable motion and the negative aerodynamic damping overcomes the positive structural damping, the amplitude of the cable motion builds up steadily in a short period of time and results in divergent motion, just as what was observed in the dynamic tests, in which the amplitude of model in-plane motion was increased from  $\pm 20$  mm to  $\pm 80$  mm within 3 minutes (Cheng, *et al.* 2002, 2003a, 2003b).

In the non-critical cases of  $\beta_s = 20^\circ$  and  $40^\circ$ , though the resultant vectors also belong to two groups in terms of the relation between their direction angles and the model yaw angle, the same angle switch phenomenon as the critical cases does not occur. Resultant vectors of Rings 2 and 3, of which the direction angles are greater when  $U = 55$  m/s, maintain the same status at  $U = 60$  m/s. Therefore, the resultant force acting at different parts of the model would not drive the cable motion in the same direction.

Analysis on the resultant force effects indicates that when the wind speed approaches to the critical range, the aerodynamic forces acting at different longitudinal locations of the cable tend to coordinate better spatially. Once the effective damping of the structure becomes negative, which means that instead of suppressing the amplitude of the motion, the damping actually contributing to its growth, and meanwhile, if a relatively larger cross-flow component is generated to continuously enhance the motion, the divergent behaviour will occur.

## 4. Span-wise correlation of lift force

### 4.1. Definition and cases

The characteristics of the cross-correlation coefficient between lift forces at various span-wise locations coinciding with different ring planes are studied in this section. The spacings between two adjacent rings starting from Rings 1 and 2 are respectively  $5.5D$ ,  $4.0D$ ,  $2.0D$  and  $D$ , where  $D$  is the model diameter. Assume  $L_i(t)$  and  $L_j(t)$  are the lift force time histories integrated from surface pressure measured by taps on Rings  $i$  and  $j$  during the whole sampling period, the lift correlation coefficient  $\rho_{ij}$  between these two time series are thus defined as  $\rho_{ij} = E[(L_i(t) - \bar{L}_i)(L_j(t) - \bar{L}_j)] / (\sigma_i \sigma_j)$ , where  $\bar{L}_k$  and  $\sigma_k$  are respectively the time average and standard deviation of lift time history  $L_k(t)$  of Ring  $k$ ,  $k=i, j$ .

Correlation coefficient of lift force within different ring planes is calculated, and its characteristics are examined for a dimensionless spacing range of  $S_{ij}/D = 1\text{--}12.5$ , where  $S_{ij}$  is the longitudinal distance between Rings  $i$  and  $j$ . Fig. 4 shows the variation of lift correlation coefficients with respect to longitudinal separation within the expected onset wind speed range of  $U = 50\text{--}60$  m/s. Each curve in these figures represents the lift correlation coefficient at a specific yaw angle. Results corresponding to both the non-critical yaw angles of  $\beta_s = 20^\circ, 40^\circ$  and the critical angles of  $\beta_s = 29^\circ\text{--}31^\circ$  are presented in the figures. It can be seen that the spatial correlation between lift forces on Rings 3 and 4 ( $S_{34}/D = 2$ ) drops significantly as compared to those between Rings 4 and 5 ( $S_{45}/$

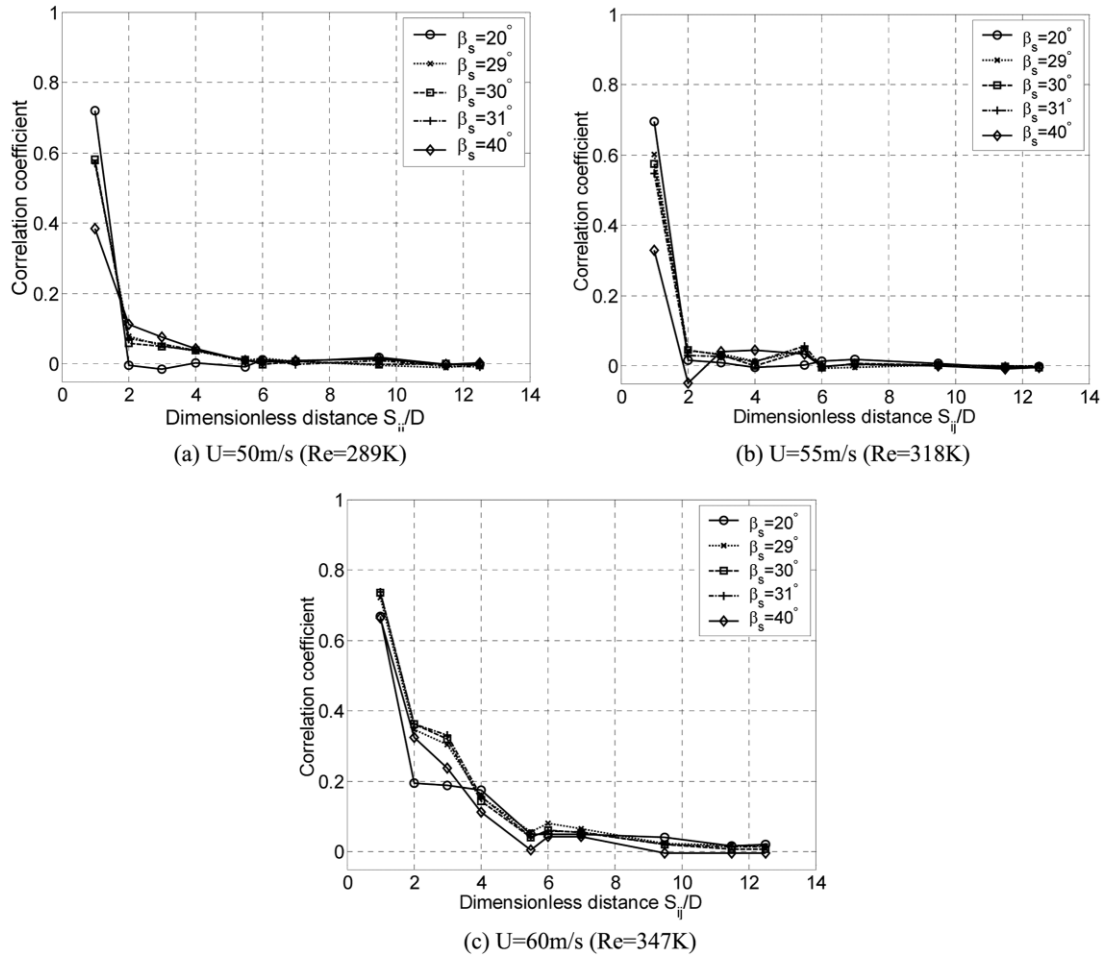


Fig. 4 Variation of lift correlation against dimensionless distance ( $\theta_s = 54.7^\circ$ )

$D = 1$ ). Once the dimensionless spacing  $S_{ij}/D$  becomes greater than 5.5, the impact of yaw angle on lift correlation is not significant. When wind speed reaches 60 m/s, lift correlation significantly increases, especially within the range of  $S_{ij}/D = 2-4$ . Also, the curves representing the cable orientation at critical yaw angles manifest the best lift correlation in the axial direction. This implies that under the critical onset conditions, flow around an inclined cable is better formed to initiate the unstable behaviour.

#### 4.2. Impact of wind speed

The impact of wind speed on the spatial correlation of lift force is depicted in Fig. 5 for dimensionless spacing of  $S_{ij}/D = 1-4$ . As shown in the figures, corresponding to different spacing, the patterns of lift correlation variation with respect to wind speed are in general similar, though with larger spacing, the correlation becomes worse as described by smaller correlation coefficients. At low wind speeds of  $U = 15-30$  m/s, which correspond to subcritical Reynolds numbers,

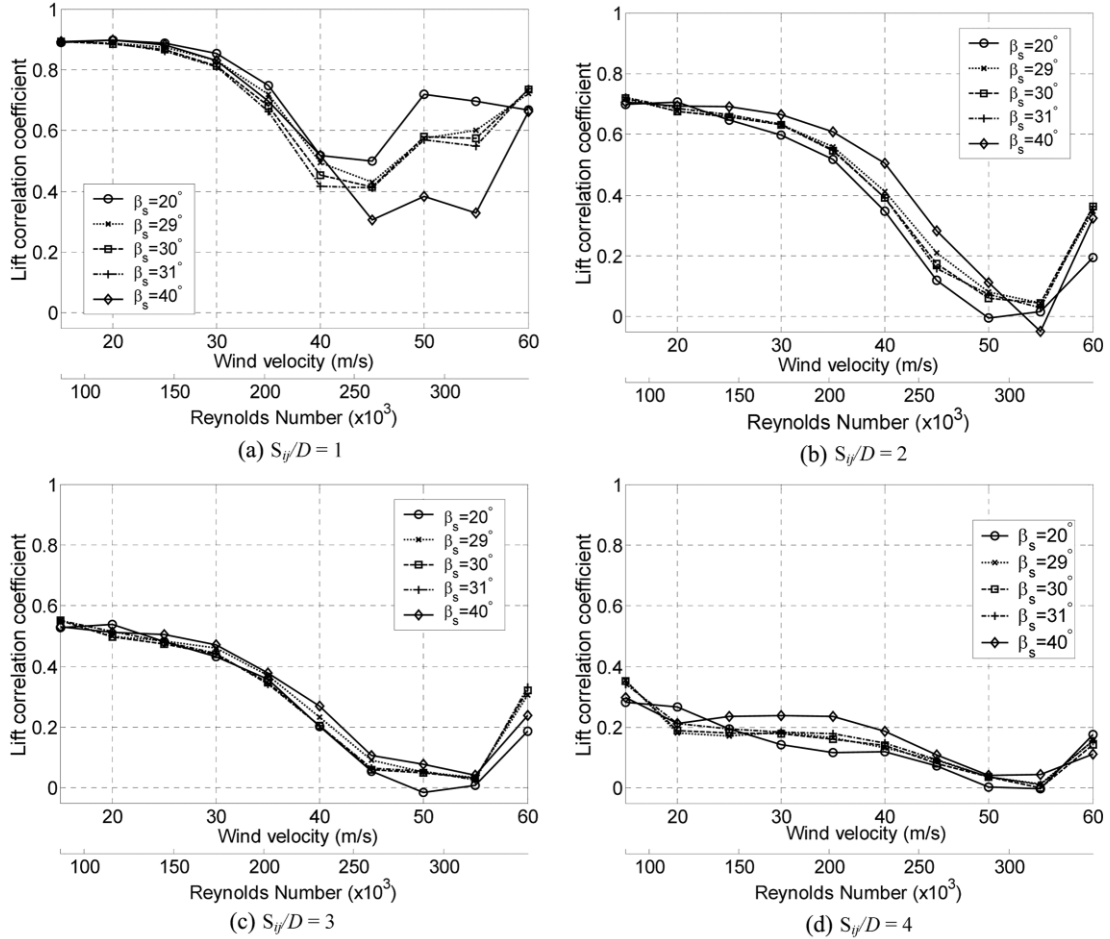


Fig. 5 Impact of wind velocity on the lift correlation ( $\theta_s = 54.7^\circ$ )

transition from laminar to turbulent state occurs along the free shear layers in the wake of the model, whereas the boundary layers remain fully laminar. Thus, lift forces at different longitudinal locations are better correlated. When wind speed approaches to the critical Reynolds number range, the transition region moves towards the separation points along the free shear layers and finally reaches the boundary layers at separation points. Flow around the inclined cable model becomes turbulent, more irregular and very sensitive to disturbances. Reflected in the figures is that the lift correlation curves start to drop rapidly. The least longitudinal lift correlation occurs in the wind velocity range of 45–55 m/s, depending on the spacing between two points along the cable axis. However, the span-wise correlation between lift forces significantly enhances when wind speed increases from 55 m/s to 60 m/s, as shown by the climbing of the curves in the figures. This is the critical wind speed range predicted by the Den Hartog criterion discussed earlier, and also agrees with the physical conditions of divergent motion observed in the dynamic tests. In terms of magnitude, the cases of which the cable model is yawed by an angle within the critical range of  $29^\circ$ – $31^\circ$  have better correlation than the non-critical cases, except when  $S_{ij}/D = 4$ , lift forces have

the best correlation when the model is yawed  $20^\circ$ . For  $S_{ij}/D = 4$ , when approach to the critical Reynolds number range, though decrease of lift correlation is not as significant as the other three cases, similar “high-drop-recovery” pattern can still be easily identified.

#### 4.3. Impact of model orientation

Under a fixed model vertical angle of  $54.7^\circ$ , the impact of model orientation in terms of yaw angle variation within the range of  $20^\circ$ – $40^\circ$  on the lift correlation at wind speeds of 40, 45, 50, 55 and 60 m/s are given in Fig. 6. This angle combination is equivalent to a cable-wind relative angle of  $57.1^\circ$ – $63.7^\circ$ . For  $S_{ij}/D = 1, 2$  and 3, in the vicinity of predicted critical yaw angle of  $30^\circ$ , the lift correlation coefficients corresponding to wind speeds of 40–55 m/s either decrease with larger yaw angle, or show concave-shaped curves; whereas those corresponding to  $U = 60$  m/s form a convex-shaped curve. This suggests that within the expected critical ranges of wind speed and yaw angle, the flow field surrounding an inclined cable becomes better organized such that the spatial

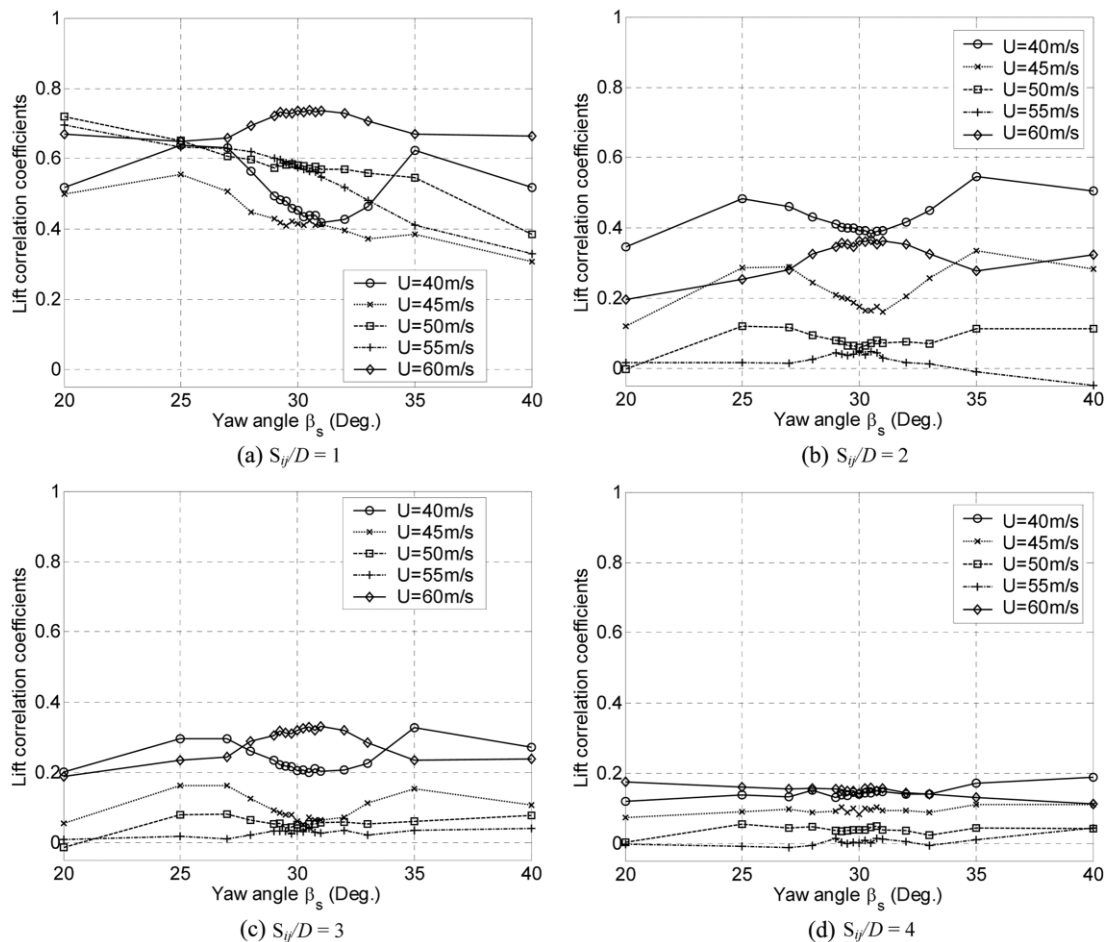


Fig. 6 Impact of yaw angle on the lift correlation ( $\theta_s = 54.7^\circ$ )

correlation of lift forces at different longitudinal locations along the cable axis is improved.

Results shown in Figs. 5 and 6 demonstrate that the ranges of wind speed and yaw angle within which the improvement of lift correlation is identified agrees with the critical conditions predicted by the Den Hartog criterion.

## 5. Spatial flow structure

To better quantify the spatial structure of flow field around an inclined cable, the cross correlation function between sampled time series of aerodynamic forces at different longitudinal locations along the model is analyzed. It is defined by  $R_{ij}(\tau) = E[A_i(t)A_j(t+\tau)]$ , where  $A_k(t)$  is the time history of lift or drag at Ring  $k$  ( $k = i, j$ ), and  $\tau$  is the time lag.

Fig. 7 presents the cross correlogram of lift and drag forces at four different wind speeds when the static model is set up at its critical orientation, i.e., inclined by  $54.7^\circ$  and yawed by  $30^\circ$ . The cross correlation function of aerodynamic forces for four different pairs of rings, i.e., Rings 2 & 3, 3 & 5, 3 & 4 and 4 & 5, are chosen for comparison.

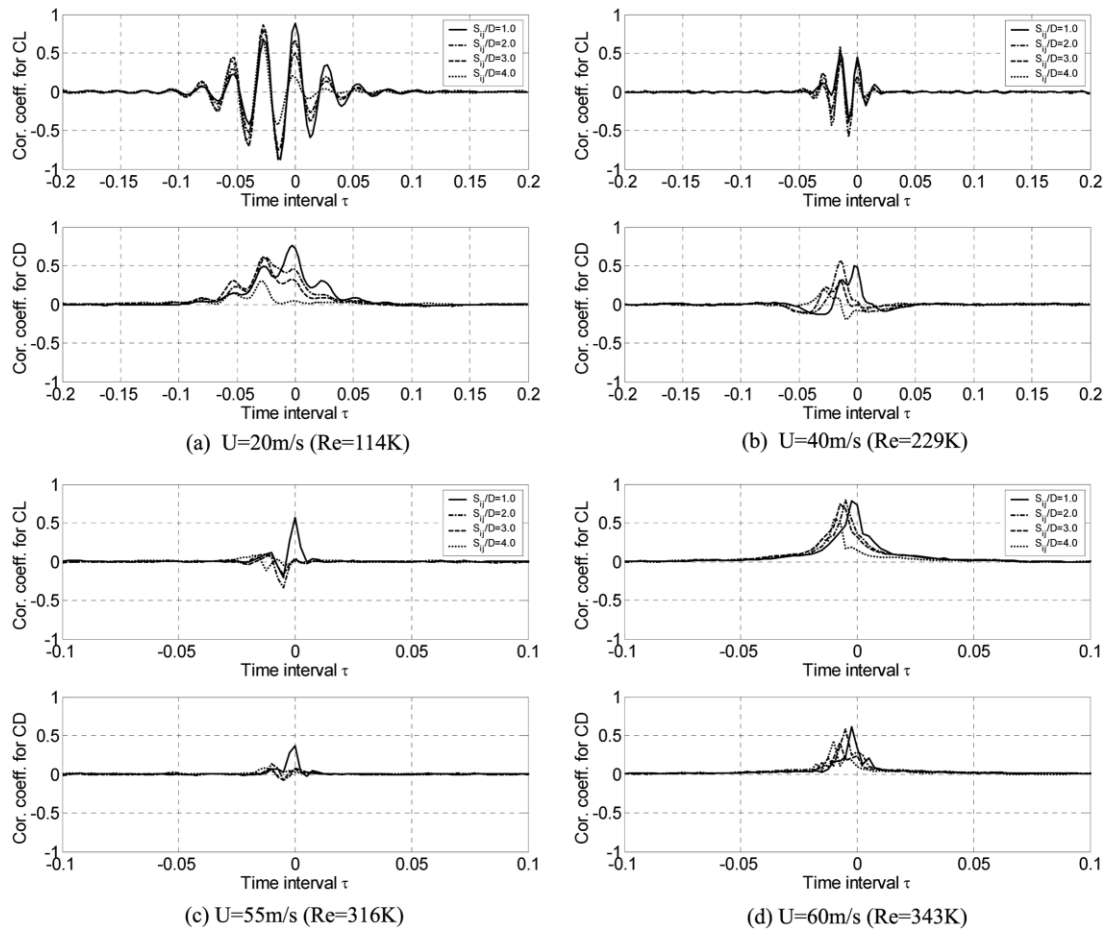


Fig. 7 Cross correlogram of aerodynamic forces ( $\theta_s = 54.7^\circ$ ,  $\beta_s = 30^\circ$ )

From Fig. 7(a), it can be seen that in the subcritical Reynolds number range, the cross correlation of lift force is governed by Kármán vortex shedding. The Strouhal number interpolated from lift correlogram is 0.164. The localized peaks of the lift and drag correlation curves correspond to each other, and the correlation of aerodynamic forces for four different spatial separations reaches localized peak at the same time. Fig. 7(b) depicts the cross correlation functions of lift and drag in the transition range from smooth to turbulent flow status. A weakened vortex shedding process with Strouhal number of 0.15 can be observed from the lift cross correlogram. The drag correlation curves, though still have localized peaks corresponding to those of lift, the best correlation for different spatial separation does not occur simultaneously. When wind speed reaches 55 m/s, flow around the model is more turbulent. As can be seen from Fig. 7(c), the spatial correlation of aerodynamic forces becomes poor, only those at a close span-wise separation of  $1.0D$  are correlated within a narrow range of time lag. However, it is interesting to note that the flow structure changes drastically with another 5 m/s increase of wind speed. Fig. 7(d) describes the spatial correlation of lift and drag at  $U = 60$  m/s, from which a systematic phase lag can be identified for both. For the same spatial separation, the lift and the drag reach the best correlation at the same time. Corresponding to the span-wise separation of  $1.0D$ ,  $2.0D$ ,  $3.0D$  and  $4.0D$ , the peak of the lift and drag correlation occurs at  $t = 0.0025$ s,  $0.005$ s,  $0.0075$ s and  $0.01$ s, respectively, which suggests the presence of the axial flow with a propagation speed of 35.6 m/s. This is comparable to the tangential component of free stream velocity, which is 34.3 m/s. The existence of axial flow alters the symmetric geometry of the model cross section. If referring to the case of ice-coated cable, of which the accretion of ice changes the symmetry of the circular cross section and results in a negative slope in the lift curve against wind angle of attack, a similar impact caused by the axial flow on the characteristics of aerodynamic forces of an inclined cable can be expected. This fact well explains the results obtained in a previous study (Cheng, *et al.* 2003b), where within the critical ranges of model orientation and wind speed, the lift force is found to have negative slope against the angle of attack. Further, it strongly supports the conclusion (Cheng, *et al.* 2003c) that the divergent galloping like motion observed on a dry inclined cable (Cheng, *et al.* 2003a) by the authors could be explained by a similar mechanism as the Den Hartog criterion.

## 6. Conclusions

Spatial structure of flow field around an inclined cable has been studied based on surface pressure measured on a stationary rigid circular cylinder model. The resultant of lift and drag forces and their spatial correlation have been examined to assist in revealing the physical nature of the dry inclined cable galloping. Results show that within the estimated critical ranges of wind speed and model orientation, flow around an inclined model is found to be better coordinated spatially. The resultant aerodynamic forces acting at different longitudinal locations along the model tend to point toward the same direction and therefore generate relatively larger cross-flow component in phase with the cable motion. The span-wise lift correlation is found to be enhanced within the critical ranges. Also, under the critical physical conditions, the existence of axial flow can be identified from the cross correlogram of both lift and drag. It would alter the symmetry of the cable cross section in a similar way as the accreted ice on power transmission lines and therefore induces negative lift slope against the angle of attack. This could be the source which excites the divergent motion of a dry inclined cable.

## Acknowledgements

This study is a result of collaborative research effort among the University of Ottawa, RWDI Inc. and NRCC, and supported by Natural Science and Engineering Research Council of Canada CRD grant. The important contributions of Dr. G.L. Larose and Mr. M.G. Savage from NRCC, Dr. J.B. Jakobsen from Stavanger University College, and Mr. C. Zurell from University of Ottawa are gratefully acknowledged.

## References

- Cheng, S. and Tanaka, H. (2002), "Aerodynamics of dry inclined cable", *The 2nd International Symposium on Advances in Wind and Structures*, Pusan, Korea, Aug. 21-23, 361-368.
- Cheng, S., Larose, G.L., Savage, M.G. and Tanaka, H. (2003a), "Aerodynamic behaviour of an inclined circular cylinder", *Wind and Structures, An Int. J.*, **6**(3), 197-208.
- Cheng, S., Irwin, P.A., Jakobsen, J.B., Lankin, J., Larose, G.L., Savage, M.G., Tanaka, H. and Zurell, C. (2003b), "Divergent motion of cables exposed to skew wind", *5th International Symposium on Cable Dynamics*, Santa Margherita, Italy, Sept. 15-18, 271-278.
- Cheng, S., Tanaka, H., Irwin, P.A. and Jakobsen, J.B. (2003c), "Aerodynamic instability of inclined cables", *5th International Symposium on Cable Dynamics*, Santa Margherita, Italy, Sept. 15-18, 69-76.
- Hikami, Y. (1986), "Rain vibrations of cables of cable stayed bridge", *J. Wind Eng., JAWE* (27) (in Japanese).
- Honda, A., Yamanaka, T., Fujiwara, T. and Saito, T. (1995), "Wind tunnel test on rain-induced vibration of the stay-cable", *Proceedings of International Symposium on Cable Dynamics*, Liège, Belgium, 255-262.
- Irwin, P.A., Nedim, A. and Telang, N. (1999), "Wind induced stay cable vibrations – A case study", *Proceedings of 3rd International Symposium Cable Aerodynamics*, Trondheim, 171-176.
- Main, J.A. and Jones, N.P. (1999), "Full-scale measurements of stay cable vibration", *Wind Engineering into the 21st Century*, Larsen, Larose & Livesey (eds), Balkema, Rotterdam, 963-970.
- Matsumoto, M., Yamagishi, M. Aoki, J. and Shiraiishi, N. (1995), "Various mechanism of inclined cable aerodynamics". *Proceeding of 9th International Conference on Wind Engineering*, New Delhi, India, 759-770.
- Matsumoto, M. (1998), "Observed behaviour of prototype cable vibration and its generation mechanism", *Bridge Aerodynamics*, Larsen & Esdahl (eds), Balkema, Rotterdam, 189-211.
- Matsumoto, M., Shirato, H., Yagi, T., Jones, N.P. and Hayashi, T. (2001), "Field observation system of cable aerodynamics in natural wind", *Proceedings of the 4th International Symposium on Cable Dynamics*, Montreal, Canada, 219-225.
- Miyata, T., Yamada, H. and Hojo, T. (1994), "Aerodynamic response of PE stay cables with pattern-indented surface", *Proceedings International Conference on Cable-stayed and Suspension Bridges (AFPC)*, Deauville, France, **2**, 515-522.
- Saito, T., Matsumoto, M. and Kitazawa, M. (1994), "Rain-wind excitation of cables of cable-stayed Higashi-Kobe Bridge and cable vibration control", *Proceedings International Conference on Cable-stayed and Suspension Bridges (AFPC)*, Deauville, France, **2**, 507-514.
- Virlogeux, M. (1998), "Cable vibrations in cable-stayed bridges", *Bridge Aerodynamics*, Balkema, 213-233.